UNIVERSIDAD
DE ANTIOQUIA

Testing the Suitability of Modified Gravity Theories for Spherical Self-gravitating Systems

Alejandra Calderon Linares

Faculty of Exact and Natural Sciences
Physics Institute
Undergraduate Program in Astronomy

Medellin, 2025

This page intentionally left blank.

UNIVERSIDAD
DE ANTIOQUIA

Testing the Suitability of Modified Gravity Theories for Spherical Self-gravitating Systems

Alejandra Calderon Linares

Professor: Juan Carlos Munoz Cuartas
Full Professor, Universidad de Antioquia

Faculty of Exact and Natural Sciences
Physics Institute
Undergraduate Program in Astronomy

Medellin, 2025

This page intentionally left blank.

Acknowledgements

First and foremost, I want to thank my dad, who allowed me to take the unconventional path of studying astronomy and who was always there with a glass of milk and an *arepa* whenever I had been working for hours. His quiet presence and small gestures made this journey lighter than it would have otherwise been. I am also grateful to my Tía and my Abuela, who reminded me again and again that giving up is not an option and who always knew how to guide me back whenever I felt lost. Together, the three of them were my constant support system, and for that I am endlessly grateful.

This thesis also owes its existence to the love and emotional support of Aleja and Meli; without you, these pages would still be nothing more than an unfinished draft gathering dust. I was equally fortunate to share this journey with the *Astrococos*, my group of friends who gave me a sense of belonging and the warmth of finding a family inside the university walls. And through it all, my pet Luna was by my side, even through sleepless nights; she is the most loyal research assistant I could have wished for.

Finally, none of this would have been complete without my professor, who became an "academic father" for me. His mentorship, filled with both scientific rigor and life lessons, left an imprint not only on this thesis but also on me as a person.

To all of you: this work is as much yours as it is mine, and I carry each of you in every page that follows.

This page intentionally left blank.

Abstract

The study of galactic dynamics has traditionally invoked dark matter to reconcile theoretical models with observations such as the flatness of galactic rotation curves. Modified Newtonian Dynamics (MOND), first proposed by Milgrom in 1983, offers an alternative by modifying gravity in the low-acceleration regime, eliminating the need for dark matter.

This thesis develops and tests a numerical framework for solving the MOND field equations, focusing on the AQUAL and QMOND formulations. A spherically symmetric Hernquist profile was adopted as the mass model, appropriate for systems ranging from galaxies to globular clusters. The gravitational potential was obtained by numerically solving Poisson's equation under both Dirichlet and Neumann boundary conditions. The code was validated against the analytical Newtonian Hernquist solution, demonstrating high accuracy and stability.

Once validated, the framework was extended to MOND. An iterative solver for AQUAL was implemented, initialized with QMOND-based estimates and refined until convergence. From the resulting potentials, dynamical observables—including circular velocity, escape velocity, and radial velocity dispersion—were derived. The results reproduce the characteristic MONDian signatures: flattened rotation curves, higher escape velocities, and enhanced dispersions in the outskirts of stellar systems.

AQUAL provides greater accuracy, while QMOND offers a computationally faster alternative, making it suitable for broad parameter-space exploration. Since the model depends only on the total mass and scale radius, it can be applied to diverse astrophysical systems, including galaxies, dwarf spheroidals, and globular clusters.

Although this work remains theoretical, the framework establishes a foundation for confronting MOND with observational data. Future applications include direct comparisons with kinematic measurements from Gaia DR3 for systems such as the Fornax dwarf galaxy and Omega Centauri, which will provide stringent tests of MOND's validity as an alternative to dark matter.

Keywords: MOND, AQUAL, QMOND, Hernquist profile, boundary conditions, Fornax Dwarf, Omega Centauri

This page intentionally left blank.

Contents

Contents vii

List of Figures xi

List of Tables xiv

1 Introduction 1
- 1.1 Problem Statement . . . 1
- 1.2 Scientific Background . . . 1
- 1.3 Research Objectives . . . 2

2 Theoretical Framework 4
- 2.1 Galactic Structure and Mass Models . . . 5
  - 2.1.1 Kinematics and Mass Distribution in Galaxies . . . 5
  - 2.1.2 The Hernquist Profile: Equations and Significance . . . 6
- 2.2 Galactic Dynamics . . . 7
  - 2.2.1 Velocity Dispersion . . . 8
  - 2.2.2 Escape Velocity . . . 8
  - 2.2.3 Rotation Curves . . . 9
  - 2.2.4 Jeans Equations . . . 9
- 2.3 Newtonian vs. MONDian Gravity . . . 10
  - 2.3.1 Newtonian Poisson's Equation . . . 10
  - 2.3.2 MOND as an Alternative to Dark Matter . . . 11
    - 2.3.2.1 QMOND (Quasilinear MOND) . . . 11
    - 2.3.2.2 AQUAL (Aquadratic Lagrangian Theory) . . . 12
    - 2.3.2.3 RAQUAL (Relativistic AQUAL) . . . 13
    - 2.3.2.4 Interpolating Functions in MOND . . . 13
    - 2.3.2.5 Phantom of RAMSES (PoR) . . . 13
    - 2.3.2.6 Comparison of MOND Models . . . 14
  - 2.3.3 External Field Effect (EFE) in MOND . . . 15
    - 2.3.3.1 EFE and isolated systems . . . 15

2.4 Summary 16

3 Methodology **17**
3.1 Suitability of Hernquist Profile as a starting point 17
3.2 Numerical Framework and Implementation 17
3.2.1 Mathematical Formulation for AQUAL 18
3.2.2 Mathematical Formulation for QMOND 19
3.2.3 AQUAL relaxation method: Implementation 19
3.2.4 Initial and Boundary Conditions 20
3.2.5 QMOND formalism 22
3.2.5.1 Numerical Solution and problem conditions 22
3.2.6 Parameter Binning and Observables 22

4 Results and Discussion **24**
4.1 Newtonian Regime 24
4.1.1 Hernquist Profile Interpretation 24
4.1.2 Solver Verification 25
4.2 Boundary and Initial Conditions 26
4.2.1 First Study Case: Galactic Object 26
4.2.1.1 Initial value problem (IVP) 26
4.2.1.2 Boundary Condition Problem (BCP) 28
4.2.1.3 MOND Observables 30
4.2.2 Parameter Exploration 31

5 Future Work and Recommendations **35**
5.1 Possible Improvements and Next Steps 35
5.2 Further Simulations and Observational Comparisons 35
5.3 Expected Comparison with Gaia DR3 36

6 Conclusion **37**

This page intentionally left blank.

List of Figures

2.1 Hubble Tuning Fork 5

3.1 Flowchart of numerical solution for AQUAL 21

4.1 Radial profiles for Hernquist model 25
4.2 Newtonian solver verification 26
4.3 IVP potential solutions 27
4.4 IVP acceleration solutions 28
4.5 BCP potential solutions 29
4.6 BCP acceleration solutions 29
4.7 Representative MOND observables 30
4.8 Potential solutions in MOND 31
4.9 Acceleration solutions in MOND 32
4.10 Rotation curves in MOND 33
4.11 Escape velocities in MOND 33
4.12 Velocity dispersion in MOND 34

This page intentionally left blank.

List of Tables

2.1 Common MOND interpolating functions and their corresponding $\nu(y)$ forms. 14
2.2 Comparison of MOND-based models and implementations. 15

This page intentionally left blank.

This page intentionally left blank.

1

Introduction

1.1 Problem Statement

Galactic dynamics have revealed significant discrepancies between the observed rotation curves of disc galaxies and the predictions derived exclusively from baryonic matter (Famaey et al., 2012). Traditionally, these differences have been addressed by introducing a dark matter halo in gravitational models. However, in 1983, Mordehai Milgrom (M. Milgrom, 1983) proposed Modified Newtonian Dynamics (MOND), an alternative that adjusts the gravitational field in low-acceleration regimes, suggesting that the observed discrepancies could be explained without invoking dark matter.

This study focuses on studying two of MOND's derived models, the AQUAL theory (J. D. Bekenstein, 2006) and the QMOND formalism (Lüghausen et al., 2014), to evaluate the ability to describe the dynamics of spherical self-gravitating systems (SGSs) under the framework of modified gravity. To properly assess these alternatives, it is essential to understand the historical development of the dark matter paradigm and the empirical challenges that motivated the emergence of MOND.

1.2 Scientific Background

The concept of dark matter was first quantitatively proposed in 1933 by Swiss astronomer Fritz Zwicky, who studied the Coma Cluster of galaxies and found that the visible matter was insufficient to account for the high random velocities of the galaxies in the cluster (Zwicky, 1933). Applying the virial theorem, Zwicky estimated that the total mass needed to gravitationally bind the cluster far exceeded the luminous matter, leading him to propose the existence of a dominant, unseen component, which he called dark matter (Andernach et al., 2017). Around the same time, Jan Oort had made similar inferences on a galactic scale from stellar motions in the Milky Way (Oort, 1932), although Zwicky's findings are generally recognized as the first strong evidence of dark matter in

galaxy clusters. This early hypothesis gained compelling support in the 1970s through the work of Vera Rubin and Kent Ford, who studied galactic rotation curves and found that the orbital velocities of stars remained constant well beyond the visible edges of galaxies, contrary to what would be expected if only visible matter were present (Rubin et al., 1978). These "flat" rotation curves implied the existence of extended dark matter halos surrounding galaxies. Together, these observations formed the basis of the dark matter hypothesis, which set forth a non-luminous and non-baryonic mass component that dominates the mass budget of galaxies and clusters. While the gravitational effects of dark matter are now evident across cosmic scales (from galaxy dynamics and gravitational lensing to the cosmic microwave background), its direct detection in laboratory experiments remains elusive despite decades of highly sensitive searches (Bertone et al., 2005; Schumann, 2019).

Since scientists have not been able to directly detect dark matter, alternative theories have been proposed to explain the observed phenomena without invoking unseen mass (Jacob D. Bekenstein, 2004). One of the most prominent is Modified Newtonian Dynamics (MOND), introduced by Milgrom, which modifies the laws of gravity in low-acceleration regimes rather than introducing additional mass (J. Bekenstein et al., 1984). MOND has been successful in explaining many galactic phenomena otherwise attributed to dark matter, such as the flat rotation curves of galaxies and the dynamics of SGSs (Famaey et al., 2012). Within MOND, different formulations exist, each with distinct mathematical treatments of the modified gravitational potential (Famaey et al., 2012; J. D. Bekenstein, 2006).

1.3 Research Objectives

The primary objective of this study is to evaluate the applicability of MOND in describing the dynamics of spherical self-gravitating systems (SGSs) and compare its predictions with those of Newtonian gravity. Specifically, this work aims to:

1. Develop a dynamic model of SGSs under both Newtonian and MONDian gravitational frameworks, using the Hernquist density profile as a density distribution model.
2. Interpret how the initial and boundary conditions change the solutions.
3. Analyze key dynamical properties such as velocity dispersion, escape velocity, and rotation curves under both gravitational theories.
4. Extend our model to different ranges of masses and scale radii, corresponding to dwarf galaxy objects.
5. Assess the viability of MOND as an alternative to dark matter in describing the internal dynamics of galaxies like the Fornax Dwarf and globular clusters, as Omega Centauri.

By achieving these objectives, this study seeks to contribute to the ongoing debate regarding the validity of alternative gravity theories and their implications for astrophysical research.

2

Theoretical Framework

2.1 Galactic Structure and Mass Models

2.1.1 Kinematics and Mass Distribution in Galaxies

The study of galactic kinematics and mass distribution provides crucial insights into the gravitational potential. Observations of galaxies suggest that the interplay between visible matter and the gravitational forces primarily determines their internal dynamics.

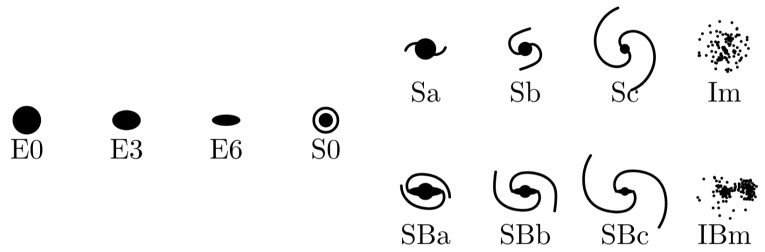

Figure 2.1: Schematic diagram of the Hubble 'tuning fork', illustrating the main galaxy morphological types (Abraham, 1998).

Galaxies are traditionally classified according to Hubble's morphological scheme (see Figure 2.1) into four main types, each exhibiting distinct kinematic properties (Mo et al., 2010):

- **Elliptical galaxies (E0–E7):** Smooth, spheroidal systems supported by random stellar motions. The subtypes of these galaxies depend on their ellipticity, defined as $10(1 - b/a)$, where a and b are the semi-major and semi-minor axes.
- **Spiral galaxies (Sa–Sc, SBa–SBc):** Rotationally supported disks with spiral arm structures. Subclasses reflect the bulge-to-disk ratio, arm tightness, and star formation activity. Their rotation curves remain flat at large radii, indicating the presence of dark matter or a need for modified gravity.
- **Lenticular galaxies (S0, SB0):** Intermediate systems with a central bulge and a disk but lacking spiral arms. They show a combination of rotation and dispersion support and little ongoing star formation.
- **Irregular galaxies (Irr):** Asymmetric systems without defined bulges or disks. Their kinematics are typically disordered and shaped by external interactions.

On the other hand, globular clusters (GCs) are compact, gravitationally bound stellar systems containing 10^4–10^6 stars in nearly spherical distributions (Binney et al., 2008). Unlike galaxies, GCs contain no gas, dust, or young stars and are generally very old, often considered relics of the early stages of galactic formation. The Milky Way hosts around 150 GCs, while large elliptical galaxies such as M87 can contain up to 10,000.

Their high central densities (typically $\sim 10^4\ M_\odot\ \mathrm{pc}^{-3}$) and spherical symmetry make GCs ideal laboratories for studying stellar dynamics and the gravitational N-body problem.

Three measures characterize typical radii: the core radius (where surface brightness drops to half the central value), the half-light radius (enclosing 50% of the total luminosity), and the tidal radius (the cluster's outer edge). While luminous GCs emit as much light as dwarf spheroidal galaxies, they are far more compact, with typical half-light radii ~ 3 pc. Some massive GCs, such as ω Centauri and G1 in M31, are suspected to be remnants of disrupted dwarf galaxies (Zhao, 2001).

Because they lack ongoing star formation, and because their stars have completed many dynamical timescales ($\sim 10^4$ orbital periods), GCs serve as the best physical realization of isolated gravitational systems (Binney et al., 2008).

The kinematics of galaxies and GCs are typically described by using:

- Velocity dispersion (σ): A measure of the random motion of stars in a galaxy, crucial for understanding dynamical equilibrium.
- Escape velocity (v_{esc}): The minimum velocity required for a star to escape the galaxy's gravitational potential, providing constraints on total mass distribution.
- Rotation curves ($v_c(r)$): The circular velocity profile as a function of radius, an essential observable for probing mass distribution.

The mass distribution in galaxies is inferred using different density profiles, which describe the spatial distribution of both stellar and dark matter components. These profiles are essential for modeling the gravitational potential and predicting dynamical behavior.

2.1.2 The Hernquist Profile: Equations and Significance

The Hernquist profile is a widely used analytical model for describing the stellar mass distribution in galaxies, particularly elliptical galaxies, globular clusters, and the bulges of spiral galaxies (Hernquist, 1990). It provides a simple yet realistic approximation to the de Vaucouleurs profile, which characterizes the surface brightness of elliptical galaxies. The Hernquist profile is notable for its central cusp and steep decline at large radii, features that make it especially suitable for modeling systems dominated by a stellar component.

Mathematically, the Hernquist density profile expresses the distribution of matter as:

$$\rho(r) = \frac{M}{2\pi}\frac{a}{r(r+a)^3}\,, \tag{2.1}$$

where M is the total mass, a is the scale radius, and r is the radial distance from the center.

The corresponding gravitational potential is:

$$\Phi(r) = -\frac{GM}{r+a}\,, \tag{2.2}$$

with G being the gravitational constant.

From this potential, we can derive the circular velocity profile as:

$$v_c(r) = \sqrt{-\frac{d\Phi}{dr}} = \sqrt{\frac{GM}{(r+a)^2}}\,. \tag{2.3}$$

This relation directly links the mass distribution to the observed kinematics of stars, allowing for comparison with observational data.

The velocity dispersion profile, which describes the spread of stellar velocities, can be obtained using the Jeans equation for a spherically symmetric system:

$$\sigma_r^2(r) = \frac{1}{\rho(r)} \int_r^\infty \rho(r') \frac{d\Phi}{dr'} dr'\,, \tag{2.4}$$

where $\sigma_r(r)$ is the radial velocity dispersion.

The Hernquist profile offers several advantages for dynamical modeling:

- It yields a finite total mass, facilitating numerical computations.
- The density falls off as r^{-4} at large radii, consistent with observed light profiles of elliptical galaxies.
- Its analytical form enables straightforward calculation of key dynamical quantities, such as circular velocity and velocity dispersion.

For these reasons, the Hernquist profile is adopted in this study to model the mass distribution of our galaxies. Its analytical tractability and physical relevance make it an effective tool for exploring the implications of both Newtonian and MONDian gravity on the system's dynamics.

2.2 Galactic Dynamics

Understanding the internal kinematics of galaxies is essential for unraveling their mass distribution and the nature of their gravitational potential. The motions of stars and gas within a galaxy are direct tracers of the underlying gravitational field, shaping key dynamical quantities, including velocity dispersion, escape velocity, and rotation curves. These observables not only provide constraints on the total mass but also serve as critical

tests for competing theories of gravity, including the dark matter paradigm and alternative theories such as MOND.

Central to the study of galactic dynamics are the Jeans equations, which link the velocity dispersion, the velocity field, and density profiles of a stellar system to its gravitational potential. This relation forms the theoretical foundation for interpreting kinematic data and constructing dynamical models of galaxies and globular clusters, such as the Fornax Galaxy and Omega Centauri. By applying the Jeans equation, one can rigorously assess how different gravitational frameworks account for the observed motions, thereby probing the validity of Newtonian gravity versus modified gravity theories in astrophysical systems.

2.2.1 Velocity Dispersion

Velocity dispersion (σ) quantifies the spread of stellar velocities around the mean motion. It is a critical parameter for studying the dynamical equilibrium of a pressure-supported collisionless system and is often used to infer the total mass distribution. The velocity dispersion tensor defines the spread of stellar velocities within a system as:

$$\sigma_{ij}^2 = \langle v_i v_j \rangle - \langle v_i \rangle \langle v_j \rangle \,, \tag{2.5}$$

where v_i and v_j are velocity components along different spatial directions. In perfectly spherically symmetric systems, we typically consider only the radial component:

$$\sigma_r^2(r) = \frac{1}{\rho(r)} \int_r^\infty \rho(r') \frac{d\Phi}{dr'} dr' \,, \tag{2.6}$$

where:

- $\rho(r)$ is the mass density,
- $\Phi(r)$ is the gravitational potential.

This equation demonstrates that velocity dispersion is directly related to the potential well of the system, indicating that variations in mass distribution have a significant impact on kinematic behavior.

2.2.2 Escape Velocity

Energy conservation provides the derivation for the escape velocity $v_{\rm esc}(r)$, which is the minimum speed a star must reach to overcome the gravitational attraction of a system and escape to infinity.

$$\frac{1}{2} v_{\rm esc}^2 + \Phi(r) = 0 \,. \tag{2.7}$$

Solving for $v_{\rm esc}$:

$$v_{\rm esc}(r) = \sqrt{-2\Phi(r)}\,. \tag{2.8}$$

For a Hernquist potential:

$$v_{\rm esc}(r) = \sqrt{\frac{2GM}{r+a}}\,; \tag{2.9}$$

where a is the scale radius. The escape velocity profile provides insights into the depth of the gravitational potential well and is often used to probe the total mass distribution in galaxies and clusters.

2.2.3 Rotation Curves

Rotation curves describe the variation of circular velocity $v_c(r)$ as a function of galactocentric radius. Observations of spiral galaxies reveal that rotation curves remain flat at large radii, contradicting the expectation from Keplerian motion, which predicts a declining rotation curve:

$$v_c^2(r) = \frac{GM}{r}\,. \tag{2.10}$$

Instead, observations suggest:

$$v_c \approx \text{constant} \quad \text{for large } r\,, \tag{2.11}$$

This discrepancy is a key motivation for the dark matter hypothesis and alternative theories, such as MOND.

For a Hernquist mass profile, the circular velocity is given by:

$$v_c(r) = \sqrt{\frac{GMr}{(r+a)^2}}\,. \tag{2.12}$$

This formula shows that the circular velocity declines at large r, making the model inconsistent with observed rotation curves unless we account for additional unseen mass.

2.2.4 Jeans Equations

The Jeans equations are fundamental relations that describe the equilibrium of a collisionless system under a gravitational potential. The radial Jeans equation in spherical symmetry is:

$$\frac{d}{dr}(\rho\sigma_r^2) + \frac{2\beta}{r}\rho\sigma_r^2 = -\rho\frac{d\Phi}{dr}\,, \tag{2.13}$$

where:

- $\beta = 1 - \frac{\sigma_t^2}{2\sigma_r^2}$ is the velocity anisotropy parameter,
- σ_t^2 and σ_r^2 are the tangential and radial velocity dispersions,
- $\rho(r)$ is the stellar density,
- $\Phi(r)$ is the gravitational potential.

For an isotropic system ($\beta = 0$), the equation simplifies to:

$$\frac{d}{dr}(\rho\sigma_r^2) = -\rho\frac{d\Phi}{dr}\,. \tag{2.14}$$

The Jeans equation is essential for deriving velocity dispersion profiles in galaxies and stellar clusters, making it a critical tool in testing gravity models.

2.3 Newtonian vs. MONDian Gravity

The fundamental challenge in galactic dynamics is explaining the observed motion of stars and gas within galaxies. Newtonian gravity predicts that rotation curves should decrease as $v_c \propto r^{-1/2}$ at large radii, yet observations indicate they remain flat. This discrepancy has traditionally been attributed to the presence of dark matter, an unknown mass component that enhances gravitational attraction.

As an alternative, Modified Newtonian Dynamics (MOND) proposes that gravity itself deviates from Newtonian predictions at low accelerations. This section explores the differences between these two frameworks by examining their governing equations and implications.

2.3.1 Newtonian Poisson's Equation

In Newtonian gravity, the potential Φ_N generated by a mass density distribution ρ satisfies Poisson's equation:

$$\nabla^2\Phi_N = 4\pi G\rho\,. \tag{2.15}$$

For a spherically symmetric system, this reduces to:

$$\frac{1}{r^2}\frac{d}{dr}\left(r^2\frac{d\Phi_N}{dr}\right) = 4\pi G\rho(r)\,. \tag{2.16}$$

The gravitational acceleration is obtained from:

$$g_N(r) = -\frac{d\Phi_N}{dr}\,. \tag{2.17}$$

For an isolated point mass M, the classical solution is:

$$\Phi_N(r) = -\frac{GM}{r}, \quad g_N(r) = \frac{GM}{r^2}, \tag{2.18}$$

In the context of galaxies, applying Newtonian gravity without accounting for additional mass results in rotation curves that decline with radius, contradicting observations.

2.3.2 MOND as an Alternative to Dark Matter

Modified Newtonian Dynamics (MOND), introduced by Milgrom (1983), proposes a modification to Newton's gravitational law in the low-acceleration regime. Instead of assuming the presence of dark matter to explain observed galactic dynamics, MOND modifies the relation between force and acceleration as:

$$\mu\left(\frac{g}{a_0}\right) g = g_N, \tag{2.19}$$

where:

- g is the MONDian acceleration,
- g_N is the Newtonian acceleration,
- $\mu(x)$ is an interpolation function,
- $a_0 \sim 1.2 \times 10^{-10}$ m/s² is the MOND acceleration scale.

For large accelerations ($g \gg a_0$), MOND reduces to Newtonian gravity. However, in the deep MOND regime ($g \ll a_0$), the effective acceleration scales as:

$$g \approx \sqrt{g_N a_0}, \tag{2.20}$$

which naturally explains the flat rotation curves in galaxies without requiring dark matter.

Although the core principle of MOND is a modification of the force law, several theoretical frameworks have been developed to cast it in a mathematically consistent form. The three most widely studied formulations are QMOND, AQUAL, and RAQUAL, each of which will be discussed in detail below.

2.3.2.1 QMOND (Quasilinear MOND)

QMOND is a simplified formulation of MOND that modifies Poisson's equation in a way that remains linear in the potential Φ (Lüghausen et al., 2014). Instead of directly altering Newton's second law, QMOND introduces a correction term to Poisson's equation:

$$\nabla^2\Phi = 4\pi G\rho + \nabla \cdot \left[\nu\left(\frac{|\nabla\Phi_N|}{a_0}\right)\nabla\Phi_N\right], \tag{2.21}$$

where $\nu(y)$ is the inverse function of the interpolation function $\mu(x)$ and Φ is the MONDian potential. The construction and physical motivation of the interpolation functions $\mu(x)$ and $\nu(y)$ will be addressed in Section 2.3.2.4, where their relevance for both AQUAL and QMOND is examined.

QMOND retains a simpler mathematical structure, making it easier to solve numerically. However, it lacks a fully developed Lagrangian formulation, making it less fundamental compared to AQUAL.

2.3.2.2 AQUAL (Aquadratic Lagrangian Theory)

AQUAL, proposed by Bekenstein & Milgrom (J. Bekenstein et al., 1984), is a more rigorous formulation of MOND, based on a modification of the Newtonian Lagrangian. Instead of modifying Newton's second law directly, AQUAL introduces a modified Poisson's equation derived from an alternative gravitational Lagrangian:

$$\mathcal{L} = -\frac{a_0^2}{8\pi G}\mathcal{F}\left(\frac{|\nabla\Phi|^2}{a_0^2}\right) + \rho\,\Phi_N\,, \tag{2.22}$$

where $\mathcal{F}(X)$ is a free function that recovers Newtonian gravity in the high-acceleration regime and MOND behavior in the low-acceleration regime. Its argument involves the squared gradient of the potential, $|\nabla\Phi|^2 = a^2$, which represents the magnitude of the gravitational acceleration expressed as a scalar. By normalizing this quantity with the MOND acceleration constant a_0, one obtains a dimensionless parameter that controls the transition between the two regimes. Using this function, the modified Poisson equation consistent with the action principle takes the form:

$$\nabla \cdot \left[\mu\left(\frac{|\nabla\Phi|}{a_0}\right)\nabla\Phi\right] = 4\pi G\rho\,. \tag{2.23}$$

Here, $\mu(x)$ is an interpolation function that smoothly transitions between the Newtonian and MOND regimes. It is important to note that for each choice of $\mu(x)$ in AQUAL, there exists a corresponding family of $\nu(y)$ functions, which are the functional inverses of $\mu(x)$. These $\nu(y)$ functions are used in QMOND as first-order approximations to the AQUAL formulation. However, it is essential to mention that not all $\nu(y)$ functions have a corresponding $\mu(x)$ function, as the latter is derived from a Lagrangian framework that ensures consistency with the action principle.

AQUAL is non-linear in Φ, which makes it more difficult to solve analytically but ensures consistency with the action principle. Our study utilizes AQUAL to solve Poisson's equation numerically for spherical systems.

2.3.2.3 RAQUAL (Relativistic AQUAL)

RAQUAL (Relativistic Aquadratic Lagrangian Theory) is an extension of AQUAL to make it compatible with General Relativity. Proposed by Bekenstein (2004), RAQUAL introduces a new scalar field ψ that modifies the metric:

$$\tilde{g}_{\alpha\beta} = e^{2\psi/c^2}(g_{\alpha\beta} + B\psi_{,\alpha}\psi_{,\beta}) \,, \tag{2.24}$$

where $g_{\alpha\beta}$ is the usual metric tensor, and B is a coupling constant. The gravitational potential in RAQUAL is modified as:

$$\Phi = \Phi_N + \psi \,, \tag{2.25}$$

where Φ is the MONDian potential, Φ_N is the Newtonian potential, and ψ is the additional scalar field component that alters gravity at large scales.

RAQUAL was developed to address MOND's lack of compatibility with relativistic frameworks, making it suitable for studying cosmology, gravitational lensing, and relativistic astrophysical systems.

2.3.2.4 Interpolating Functions in MOND

The Modified Newtonian Dynamics (MOND) framework relies on interpolating functions that ensure a smooth transition between the Newtonian and deep-MOND regimes. In AQUAL, the interpolation is introduced via a function $\mu(x)$, where $x = |\nabla\Phi|/a_0$, while in QMOND the relevant function is $\nu(y)$, where $y = |\nabla\Phi_N|/a_0$. These functions satisfy:

$$\mu(x) \to 1 \quad \text{for } x \gg 1, \quad \text{and} \quad \mu(x) \to x \quad \text{for } x \ll 1 \,; \tag{2.26}$$

$$\nu(y) \to 1 \quad \text{for } y \gg 1, \quad \text{and} \quad \nu(y) \to y^{-1/2} \quad \text{for } y \ll 1 \,. \tag{2.27}$$

Several families of interpolating functions are commonly used. Table 2.1 summarizes their functional forms and properties.

2.3.2.5 Phantom of RAMSES (PoR)

The Phantom of RAMSES (PoR) code displays a numerical implementation of Milgromian dynamics. It adopts the formal QMOND formulation of MOND by modifying the Poisson equation to include MOND effects via an interpolation function $\nu(y)$. The core equation solved by PoR, and also used in this work for analytical development, is:

$$\nabla^2\Phi(r) = 4\pi G \left(\rho_{\rm b}(r) + \rho_{\rm ph}(r)\right) \,, \tag{2.28}$$

with a phantom density $\rho_{\rm ph}(r)$ given by:

Table 2.1: Common MOND interpolating functions and their corresponding $\nu(y)$ forms.

Name	$\mu(x)$	$\nu(y)$
Simple ($n = 1$)	$\dfrac{x}{1+x}$	$\dfrac{1+\sqrt{1+4y^{-1}}}{2}$
Standard ($n = 2$)	$\dfrac{x}{\sqrt{1+x^2}}$	$\left[\dfrac{1+\sqrt{1+4y^{-2}}}{2}\right]^{1/2}$
n-family	$\dfrac{x}{(1+x^n)^{1/n}}$	$\left[\dfrac{1+\sqrt{1+4y^{-n}}}{2}\right]^{1/n}$
α-family	$\dfrac{2x}{1+(2-\alpha)x+\sqrt{(1-\alpha x)^2+4x}}$	No simple expression
Exponential (β)	–	$(1-e^{-y})^{-1/2}+\beta e^{-y}$
γ-family	–	$(1-e^{-y^\gamma/2})^{-1/\gamma}+(1-\gamma^{-1})e^{-y^\gamma/2}$
δ-family	–	$(1-e^{-y^\delta/2})^{-1/\delta}$

$$\rho_{\rm ph}(r) = \frac{\nabla\cdot\left[\nu\left(|\nabla\phi(r)|/a_0\right)\nabla\phi(r)\right]}{4\pi G}\,. \tag{2.29}$$

In other words, the total gravitational potential, $\Phi = \Phi_N + \Phi_{\rm ph}$, can be divided into two parts: a classical (Newtonian) part, Φ_N, and an additional Milgromian part, $\Phi_{\rm ph}$. The additional matter density distribution, $\rho_{\rm ph}(r)$, that would, in Newtonian gravity, yield the additional potential $\Phi_{\rm ph}(r)$, and is known as the *phantom dark matter* (PDM) density.

This formulation enables the computation of the MOND potential solely from the baryonic mass distribution, without invoking dark matter halos, which leads to a decomposition of the equation into two terms: a Newtonian component derived from the baryonic profile, and a MOND correction term. In this thesis, the above equation is analytically developed under spherical symmetry, using a Hernquist profile for $\rho(r)$.

The use of this formulation is motivated by its applicability to both numerical simulations, such as those performed with PoR, and semi-analytic treatments like the one developed here for spherical systems, including the Fornax Dwarf and Omega Centauri.

2.3.2.6 Comparison of MOND Models

Let's see how the different MOND models compare in terms of their formulation, advantages, and limitations:

In summary, MOND provides a compelling alternative to dark matter by modifying the gravitational force law at low accelerations. The different formulations of MOND offer various advantages and limitations: QMOND is computationally efficient and suitable for symmetric systems, while AQUAL is more fundamental and better suited for

Model	Description	Equation	Advantages	Limitations
QMOND	Linear formulation of MOND	$\nabla^2\Phi = 4\pi G\rho + \nabla \cdot (\nu \nabla \Phi_N)$	Computationally simpler	Lacks a fundamental $\mathcal{L}$
AQUAL	Nonlinear $\mathcal{L}$-based MOND	$\nabla \cdot (\mu \nabla \Phi) = 4\pi G\rho$	More fundamental and consistent	Harder to solve numerically
RAQUAL	Relativistic version of AQUAL	$\Phi = \Phi_N + \psi$	Compatible with General Relativity	Complexity, not widely tested

Table 2.2: Comparison of MOND-based models and implementations.

theoretical consistency. RAQUAL extends MOND into a relativistic regime, enabling applications in cosmology and gravitational lensing. Additionally, Phantom of RAMSES (POR) bridges the gap between theory and simulation by implementing QMOND within a numerical framework, enabling realistic galaxy simulations that utilize only baryonic matter. This research applies AQUAL and QMOND to solve Poisson's equation numerically and test MOND against Omega Centauri's kinematics.

2.3.3 External Field Effect (EFE) in MOND

A key distinction between MOND and Newtonian gravity is the External Field Effect (EFE), which arises because MOND is a non-linear theory. Unlike Newtonian gravity, MONDian subsystems cannot be treated independently from the external gravitational field they experience.

In Newtonian mechanics, an object in an external uniform gravitational field g_{ext} does not affect its internal dynamics. However, in MOND, the presence of g_{ext} modifies the system's internal gravity (Mordehai Milgrom, 2009):

- When $g_{\text{int}} \gg g_{\text{ext}}$, the system behaves as expected in MOND.
- When $g_{\text{int}} \ll g_{\text{ext}}$, the system reverts to Newtonian dynamics.

This effect is observable in galaxy clusters and the Solar System, where the influence of the Milky Way's external acceleration can suppress MONDian effects.

2.3.3.1 EFE and isolated systems

This study initially considered whether we needed to include the EFE when modeling spherical self-gravitating systems, such as Omega Centauri. A review of the literature suggested that, for systems sufficiently isolated from external gravitational fields, the external acceleration can be regarded as negligible, and the EFE does not need to be incorporated into the final MONDian model.

2.4 Summary

The study of galactic dynamics has progressed from the initial discovery of mass discrepancies in galaxies to the development of both dark matter and modified gravity theories. While Newtonian gravity requires the introduction of unseen mass to account for flat rotation curves and high velocity dispersions, MOND, especially in its AQUAL formulation, offers an alternative by modifying the gravitational force law at low accelerations. This approach provides a self-consistent explanation for many observed galactic phenomena without invoking dark matter, highlighting the importance of testing such frameworks in systems like the Fornax Dwarf and Omega Centauri.

Key distinctions between the two theories include:

- Newtonian gravity follows Poisson's equation and requires dark matter.
- MOND modifies the force law, introducing the characteristic acceleration a_0.
- The External Field Effect (EFE) in MOND connects internal system dynamics with external gravitational influences.

3

Methodology

In this chapter, we present the methodology adopted to study the dynamics of spherical systems under the Modified Newtonian Dynamics (MOND) framework. We begin by justifying the choice of the Hernquist profile as a suitable initial condition for our models. Then, we detail the numerical framework developed to solve the AQUAL equation and its QMOND approximation, including the implementation of boundary and initial conditions, numerical integration methods, and convergence criteria. The methodology also compares these solutions with the QMOND used on the Phantom of RAMSES, ensuring consistency between different MOND formulations.

Finally, we derived physical observables, including circular velocity, escape velocity, and velocity dispersion, from the models. We employed them as the basis for a systematic comparison and evaluation of the different MONDian implementations.

3.1 Suitability of Hernquist Profile as a starting point

Before delving into the numerical methods, we first justified the choice of the Hernquist profile as a suitable starting point for our models. For that purpose, we studied the density, potential, acceleration, velocity profiles, and velocity dispersion within a range of scale radii. After conducting this analysis, we can then test our pipeline using Newtonian gravity, a necessary step before implementing the MONDian framework.

3.2 Numerical Framework and Implementation

For this work, we implemented a numerical framework to solve the AQUAL equation in the context of MOND. To validate the model, we compared it with the QMOND formalism to ensure consistency. We also compared it with the Newtonian model, as they should be similar in high-acceleration regimes. Let's examine the implementation of the numerical framework step by step.

3.2.1 Mathematical Formulation for AQUAL

Starting from eq. (2.23), the AQUAL equation can be expressed as

$$\frac{d^2\Phi_M}{dr^2} = \frac{4\pi G\rho_r}{\mu} - \left(\frac{1}{\mu}\frac{d\mu}{dr} + \frac{2}{r}\right)\frac{d\Phi_M}{dr}\,, \tag{3.1}$$

where the interpolating function μ is defined as

$$\mu(x) = \frac{x}{\sqrt{1+x}}\,, \tag{3.2}$$

with $x = a/a_0$, the ratio of the local acceleration to the MOND acceleration constant.

The choice of this interpolation function is motivated by the fact that it admits a corresponding $\nu(y)$ (see Table 2.1), which will later prove convenient.

Expanding Eq. (3.1) explicitly in terms of the system parameters—the mass M, scale radius a, MOND acceleration a_M, MOND acceleration constant a_0, and radial distance r—the AQUAL equation becomes

$$\begin{aligned}\frac{d^2\Phi_M}{dr^2} = {} & 2GM\,\frac{a}{r}\,\frac{1}{(r+a)^3}\,\frac{a_0}{a_M}\left(1+\frac{a_M}{a_0}\right) \\ & - \left[\frac{a_0}{a_M}\left(1+\frac{a_M}{a_0}\right)\frac{a_0}{(a_M+a_0)^2}\,\frac{da_M}{dr} + \frac{2}{r}\right]\frac{d\Phi_M}{dr}\,.\end{aligned} \tag{3.3}$$

Since the AQUAL formalism requires knowledge of the MONDian acceleration a_M, an auxiliary relation is necessary to provide an initial approximation. At this stage, the QMOND approach becomes useful, as it modifies the Newtonian acceleration directly through the relation

$$a_M = \nu(y)\,a_N\,, \tag{3.4}$$

where the function $\nu(y)$ associated with Eq. (3.2) is

$$\nu(y) = \frac{1+\sqrt{1+4y^{-1}}}{2}\,, \tag{3.5}$$

with $y = a_0/a_N$, the ratio of the MOND acceleration constant to the Newtonian acceleration.

Substituting eq. (3.5) into eq. (3.4) and solving for the potential leads to the QMOND-approximated form of the AQUAL equation:

$$\frac{d^2\Phi_M}{dr^2} = 4\pi G\rho_N(r)\,\nu(r) - \left[\nu(r)\frac{d\nu^{-1}}{da_N}\frac{da_N}{dr} + \frac{2}{r}\right]\frac{d\Phi_M}{dr} \tag{3.6}$$

Expressing Eq. (3.6) explicitly in terms of the object's mass M, scale radius a, MOND acceleration constant a_0, and radial distance r, we obtain

$$\frac{d^2\Phi_M}{dr^2} = \frac{GMa}{r(r+a)^3}\left(1+\sqrt{1+\frac{4a_0}{a_N}}\right) - \left[\frac{2a_0}{a_N^2}\left(1+\sqrt{1+\frac{4a_0}{a_N}}\right)^{-1}\left(1+\frac{4a_0}{a_N}\right)^{-1/2}\frac{da_N}{dr}+\frac{2}{r}\right]\frac{d\Phi_M}{dr}\,. \tag{3.7}$$

To numerically solve Eq. (3.7), we employ a relaxation method—an iterative procedure that refines the potential Φ until convergence is achieved. The details of this implementation are described in Section 3.2.3. Before addressing the numerical implementation, we present the QMOND formalism, which serves as a complementary counterpart to AQUAL and enables direct comparison for consistency verification.

3.2.2 Mathematical Formulation for QMOND

Starting from Eq. (2.21) and adopting the same interpolating function $\nu(y)$ given in Eq. (3.5), we obtain

$$\frac{d^2\Phi_M}{dr^2} = \frac{2GMa}{r(r+a)^3}(\nu+1) + \frac{2a_0}{a_N^2}\frac{1}{\sqrt{1+\frac{4a_0}{a_N}}}\left(\frac{GM}{(r+a)^3}\right)^2(r+a) - \frac{2}{r}\frac{d\Phi_M}{dr}\,. \tag{3.8}$$

Unlike AQUAL, the QMOND formalism does not require a relaxation scheme. This is because the modification to the Newtonian acceleration introduced by $\nu(y)$ provides a direct solution, eliminating the need for iteration. Having established both formulations, we now proceed to describe the relaxation method applied to Eq. (3.3).

3.2.3 AQUAL relaxation method: Implementation

A reliable implementation of the AQUAL formalism requires accurate evaluation of the derivatives of the QMOND-based potential approximation before their substitution into the AQUAL equation. To achieve this, we employ five-point finite difference schemes, together with midpoint and endpoint formulas, which strike an effective balance between numerical accuracy and computational efficiency. The central and forward finite difference approximations are given, respectively, by

$$\frac{df(r)}{dr} = \frac{1}{12\Delta r}\left[f(r-2\Delta r) - 8f(r-\Delta r) + 8f(r+\Delta r) - f(r+2\Delta r)\right] \tag{3.9}$$

and

$$\frac{df(r)}{dr} = \frac{1}{12\Delta r}\Big[-25f(r) + 48f(r+\Delta r) - 36f(r+2\Delta r) + 16f(r+3\Delta r) - 3f(r+4\Delta r)\Big]. \tag{3.10}$$

The relaxation scheme begins with an initial guess for the potential, obtained from the QMOND approximation (Eq. 3.8). At each iteration, the derivatives are evaluated, the solution is updated, and the result is interpolated using linear splines. Convergence is assessed through the root mean square (RMS) error between successive iterations. The procedure continues until the RMS error falls below the prescribed tolerance of 0.01%, thereby ensuring both accuracy and numerical stability in the MOND potential.

The connection between the AQUAL formulation and the QMOND-based approximation, together with the corresponding iterative procedure, is summarized in Figure 3.1.

3.2.4 Initial and Boundary Conditions

To solve these equations, we considered both initial and boundary conditions, each tailored to ensure physically meaningful solutions in the MOND and Newtonian regimes. A key boundary condition, following (Famaey et al., 2012), is imposed at infinity for the potential:

$$\Phi_M|_\infty = \sqrt{GMa_0}\ln r, \tag{3.11}$$

which reflects the expected asymptotic behavior in the MOND regime and does not necessarily coincide with the Newtonian case at the origin. For the acceleration, two types of conditions are used depending on the problem setup:

There are two types of boundary conditions applied to the MOND acceleration:

- **At the origin:** The MONDian acceleration must match the Newtonian value,

$$\left.\frac{\partial\Phi_M}{\partial r}\right|_{r=0} = \left.\frac{\partial\Phi_N}{\partial r}\right|_{r=0}. \tag{3.12}$$

- **At infinity:** The MONDian potential must recover the expected asymptotic behavior,

$$\left.\frac{\partial\Phi_M}{\partial r}\right|_{r\to\infty} = \sqrt{GMa_0}\,\frac{1}{r}. \tag{3.13}$$

The initial value problem, defined with conditions at infinity and integrated from infinity to zero, uses the `odeint` function from `scipy.integrate` to find the solution. The boundary value problem, defined with conditions at both the origin and

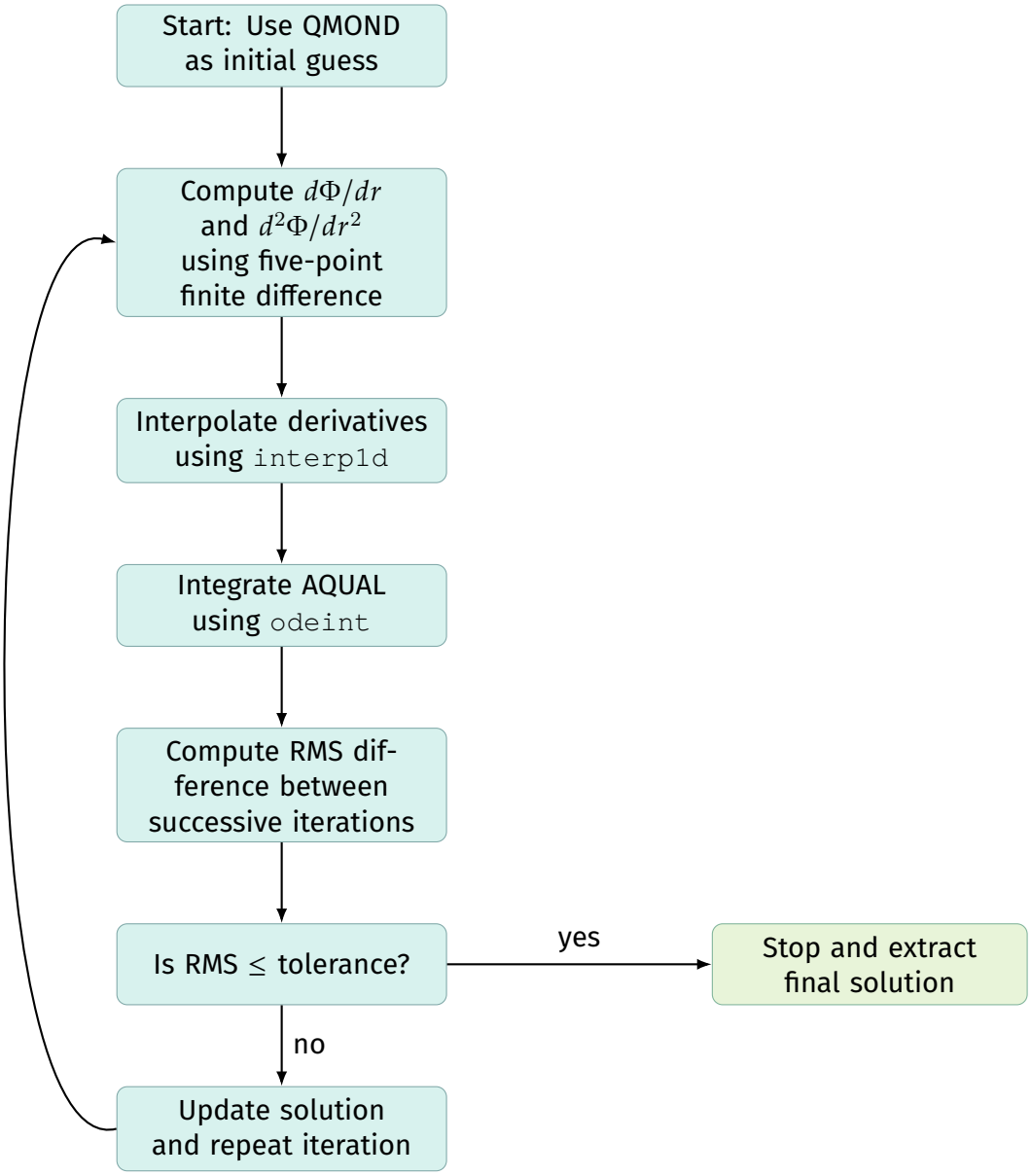

Figure 3.1: Flowchart of the iterative numerical scheme used to solve the AQUAL equation.

infinity, employs the `solve_bvp` function from the same module. Careful selection of these conditions ensures that the numerical solutions transition smoothly between the Newtonian and MOND regimes while maintaining physical consistency across the entire radial range.

Numerical integration employs the `odeint` function from the `scipy.integrate` module, which efficiently solves ordinary differential equations (ODEs) in Python. The QMOND-approximation (2.21) solution provides the initial conditions, and the AQUAL iterative process continues until the specified convergence criterion is satisfied.

Once the solution converges, the resulting AQUAL solution is compared directly with the QMOND approximation. Both solutions agree within a few percent, which supports the use of the QMOND approach in subsequent analyses due to its computational efficiency and comparable accuracy.

3.2.5 QMOND formalism

To ensure consistency with the AQUAL-QMOND approach, we used the same interpolating function $\nu(y)$, adopting the simple $n = 1$ form, which allows for a direct and meaningful comparison between the two methods.

3.2.5.1 Numerical Solution and problem conditions

The QMOND-based solution relies on Newtonian acceleration, eliminating the need for an iterative relaxation method. For consistency with the AQUAL approach, we applied the same initial and boundary conditions, and employed the corresponding `SciPy` integration functions. Using identical conditions and numerical tools allows a direct and meaningful comparison of the resulting potentials and observables from both methods.

3.2.6 Parameter Binning and Observables

As we saw in section 2.2, we can derive the observables from the potential solution and the corresponding acceleration for a fixed pair of values $M = 10^{11}\, M_\odot$ and $a = 2.0$ pc, according to the following expressions:

- $v_c(r) = \sqrt{r\,\frac{d\Phi}{dr}}$ (circular velocity)
- $v_{\rm esc}(r) = \sqrt{2|\Phi(r)|}$ (escape velocity)
- $\sigma_r(r)$ (from the isotropic Jeans equation)

The Jeans equation provides the theoretical framework for deriving the radial velocity dispersion $\sigma_r(r)$, establishing a link between the underlying gravitational potential

and the kinematic properties of the system. The complete derivation appears in the Results and Discussion chapter. The numerical integration of the boundary-value problem extends to $r = 200.0a$. In contrast, the initial-value problem, defined at infinity, was extended to $r = 2000a$ to represent the asymptotic boundary condition more accurately.

Then, the potential and acceleration were interpolated onto a uniform grid with resolution $\Delta r = 10^{-2}$ kpc over the range $[0, 10]$ kpc for different (M, a) parameter pairs. This approach enables a systematic analysis of trends in the solutions by investigating the dependence of the solutions on mass and scale radius. The computations cover the following parameter ranges:

- Masses $M \in [10^9, 10^{11}]\, M_\odot$, in 10 bins spaced by 0.22 dex.
- Scale radii $a \in [6, 12]$ kpc, in 4 bins spaced by 2 kpc.

The study adopts these parameter ranges because they represent typical masses and scale radii observed in spherical systems such as galaxies, enabling a comprehensive exploration of MONDian dynamics across different ranges.

The sets of curves in mass M, evaluated for different scale radii a, confirm that the solutions remain consistent across the explored ranges, which reinforces the robustness of the results. At the same time, the variation in (M, a) primarily changes the values of the curves without altering the overall form of the solutions. The subsequent chapter provides a detailed presentation of these results.

4

Results and Discussion

This chapter presents the analysis of spherical self-gravitating systems under both Newtonian gravity and Modified Newtonian Dynamics (MOND). Several computational strategies were tested; some produced inconsistent or unstable outcomes and are in the annexes, while others provided robust and interpretable results. The analysis focuses on four main components: the Hernquist profile, the treatment of boundary conditions (both Neumann and Dirichlet), the iterative AQUAL solution and the QMOND solution, and the parametric exploration carried out for both MONDian frameworks.

We begin by examining the Newtonian regime.

4.1 Newtonian Regime

We first validated our numerical framework in the Newtonian case. The Hernquist profile served as the reference mass distribution and provided a benchmark to test the solver against known analytical solutions. Let's delve into the characteristics of this profile.

4.1.1 Hernquist Profile Interpretation

The Hernquist profile describes a spherically symmetric mass distribution and is a useful model in both Newtonian and MONDian contexts. In the Newtonian case, decreasing the scale radius a deepens the central potential, steepens the gradients, and increases orbital velocities and dispersions, as shown in Figure 4.1.

The lower-left panel of Figure 4.1 shows that, at small radii ($r \ll a$), the velocity dispersion follows the trend $\sigma_r^2(r) \sim r\ln(r)$. On the other hand, at large radii ($r \gg a$), it decreases as $\sigma_r^2(r) \sim r^{-1}$. These behaviors are consistent with expectations for a Keplerian potential and highlight the limitations of Newtonian gravity, motivating the study of MONDian dynamics. Overall, the Hernquist model provides a reliable description of the systems considered in this work. In the next subsection, we are going to explain how we solve the Poisson equation, using this density profile.

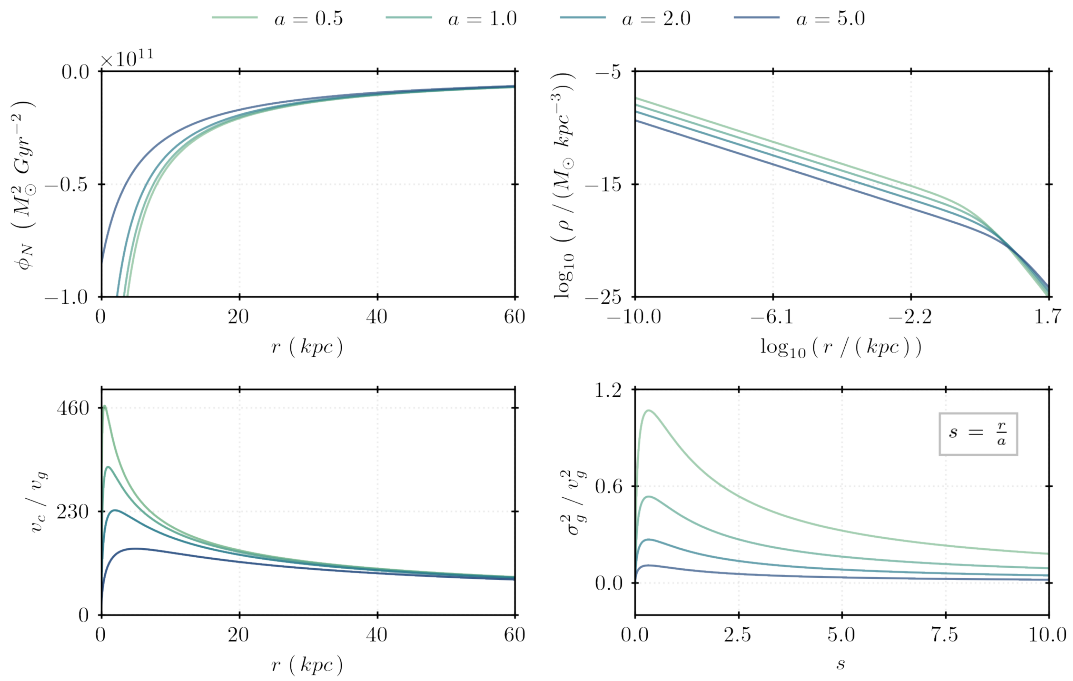

Figure 4.1: Radial profiles for the Hernquist model.
Gravitational potential $\phi(r)$, density $\rho(r)$, circular velocity $v_c(r)$, and velocity dispersion $\sigma_r(r)$, computed with a total mass $M = 10^{11}\,M_\odot$ and scale radii $a = 0.5,\ 1.0,\ 2.0,\ 5.0$ kpc. All profiles were calculated on a grid with $Nr = 10000$ points and $r_{\max} = 60$ kpc to ensure high resolution.

4.1.2 Solver Verification

We used the `odeint` function to solve the Newtonian Poisson equation under both Neumann and Dirichlet boundary conditions, where the potential and its first derivative are fixed at ($r \to \infty$). The solver was efficient and reproduced the analytical Hernquist solution with high precision. The mean relative error was 1.35×10^{-7} for the potential and 3.42×10^{-7} for the acceleration. As shown in Figure 4.2, the numerical and analytical solutions overlap completely, while the relative error across the entire radial range remains between 10^{-9} and 10^{-5}, with slightly larger errors at the center.

These results demonstrate that the numerical solver achieves accuracy, precision, and stability, making it a reliable tool for more complex gravitational models. Having confirmed the solver's reliability in the Newtonian framework, we now turn to the role of boundary conditions in shaping the MONDian solutions.

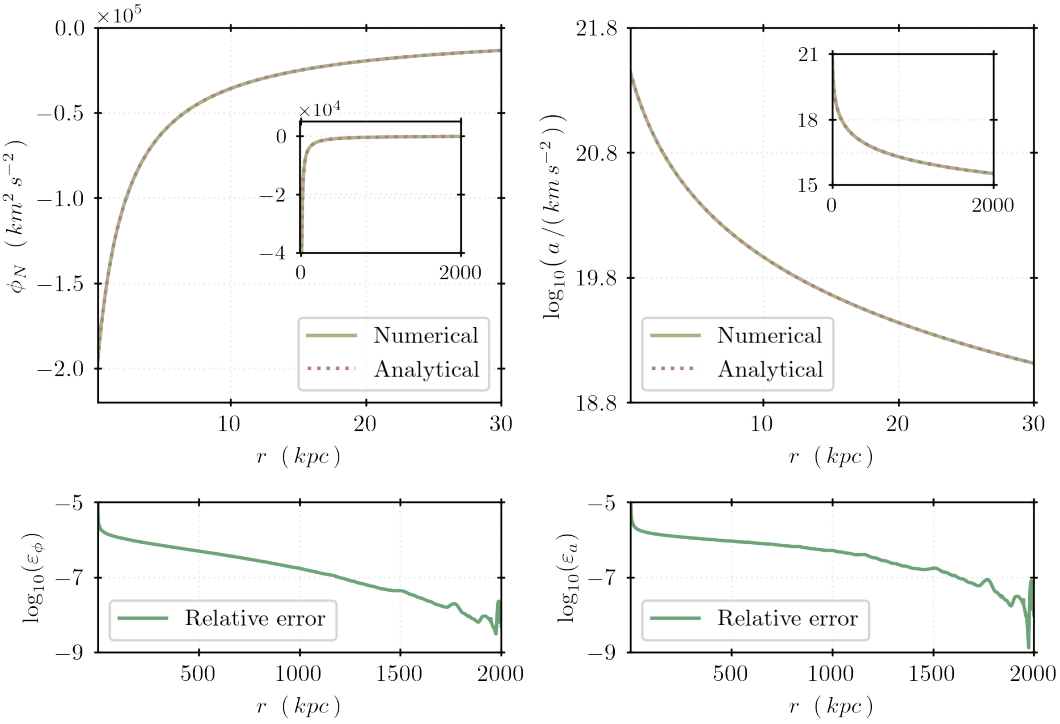

Figure 4.2: Verification of the Newtonian solver using `odeint`.
Top panels: gravitational potential (left) and acceleration (right) obtained numerically and compared with the analytical Hernquist solution. **Bottom panels:** relative errors between numerical and analytical solutions.

4.2 Boundary and Initial Conditions

4.2.1 First Study Case: Galactic Object

4.2.1.1 Initial value problem (IVP)

The first MONDian formulation we implemented was AQUAL (equation). For the fiducial test case, the solver converged after 1961 iterations, reaching a final RMS difference of 0.01%. We compared the solution with the zeroth-order approximation (AQUAL0) and found them statistically indistinguishable. This agreement is expected given the idealized nature of our setup—spherical symmetry and the absence of the External Field Effect (EFE). While more complex systems may introduce significant differences, in this context, the approximation allowed us to compute the remainder of our study efficiently without a prohibitive computational cost.

We first examined the AQUAL equation as an initial value problem (IVP), with conditions (3.11) and (3.13). Since the conditions were imposed at $r \to \infty$, the system had more freedom: the solution could vary significantly as it propagated inward toward the center. Figures 4.3 and 4.4 illustrate these consequences. The resulting profiles do not

strictly reproduce the Newtonian potential, though they follow its general trend. The QMOND IVP solution, however, diverges sharply at small radii, failing to satisfy the requirement that MOND should recover Newtonian behavior in the high-acceleration regime.

The lower panel of Figure 4.3 compares MONDian and Newtonian potentials. Both MOND formulations enhance the potential by nearly the same factor over most of the integration range, with visible discrepancies only between $r \sim 0$ and $r \sim 10$. The AQUAL comparison, however, shows a non-smooth profile with a sharp minimum between the origin and $r = 5$. This occurs because the potential begins negative and becomes positive at that point.

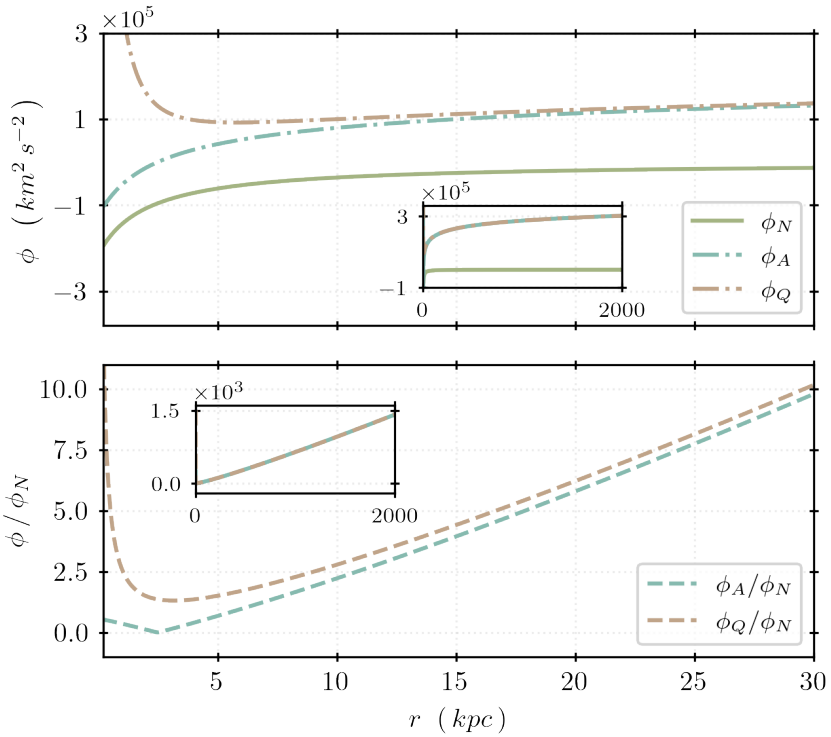

Figure 4.3: Potential solutions obtained with `odeint` under initial value conditions, for both AQUAL and QMOND. The inset plots display the full integration range.

The acceleration profiles reveal complementary trends. For QMOND, the solution is non-smooth: the acceleration grows rapidly for r close to the center, decreases until $r \sim 5$ kpc to 10 kpc, and then increases again, exceeding the Newtonian acceleration around $r \sim 11$ kpc. This behavior reflects the role of the interpolation function, which enhances acceleration in the system's outskirts. By contrast, the AQUAL acceleration increases monotonically from the center, converging to the QMOND profile at large radii, as both are constrained to match at infinity.

These first solutions demonstrate that the model is internally consistent. Although QMOND fails to reproduce the expected Newtonian behavior at small radii, both ap-

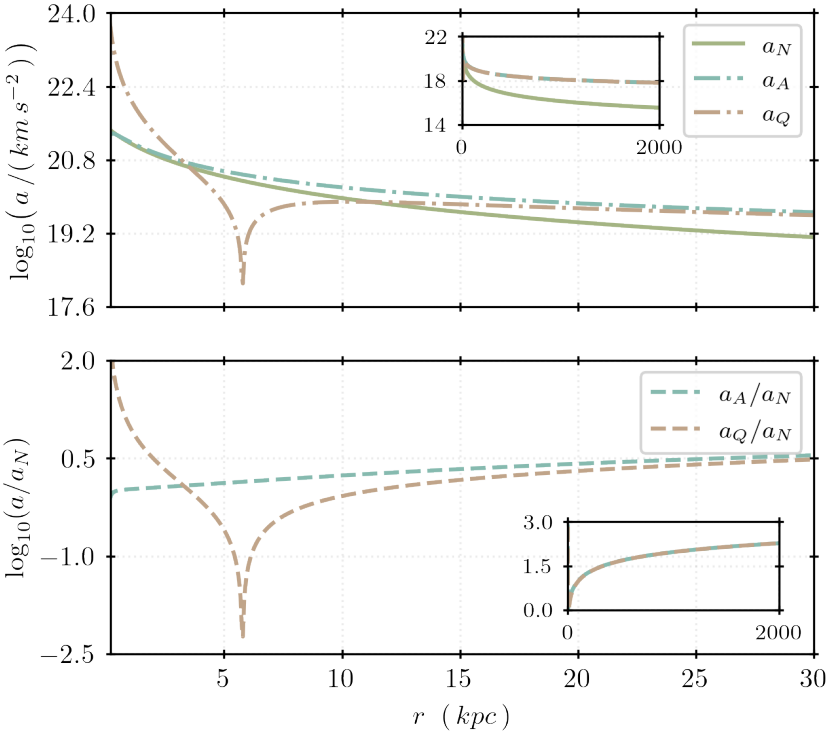

Figure 4.4: Acceleration obtained with `odeint` under initial value conditions, for both AQUAL and QMOND. The inset plots display the full integration range.

proaches converge to similar profiles at large radii. To mitigate the spurious central behavior in QMOND and enforce Newtonian consistency at small radii, we next explored boundary value conditions.

4.2.1.2 Boundary Condition Problem (BCP)

Figures 4.5 and 4.6 present the results obtained by solving the Poisson equation under boundary conditions using `solve_bvp`. In this formulation, conditions are imposed at the center on the modified acceleration.

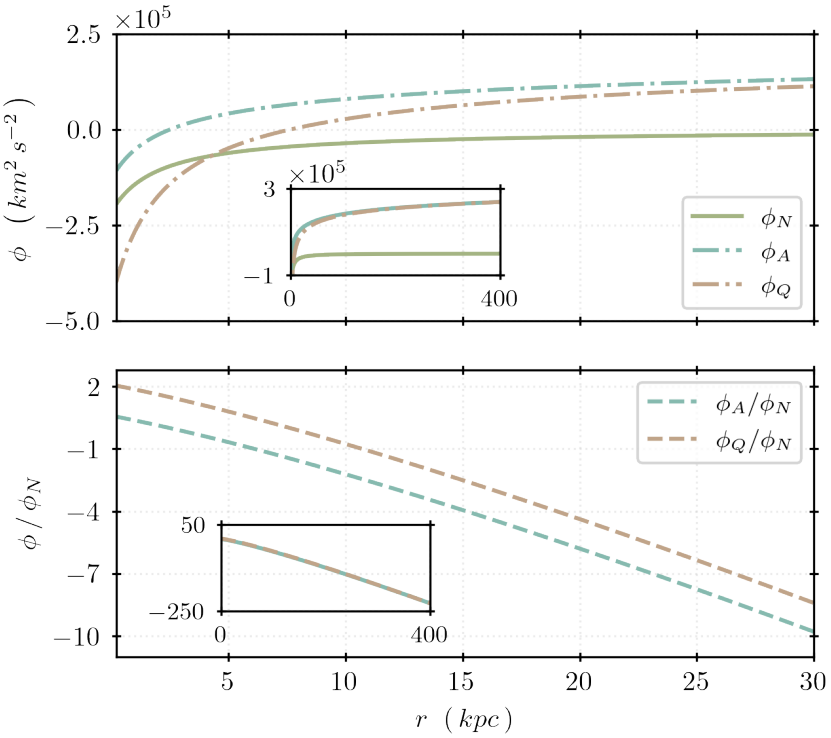

Figure 4.5: Potential obtained with `solve_bvp` under boundary value conditions, compared with the analytical Hernquist potential.

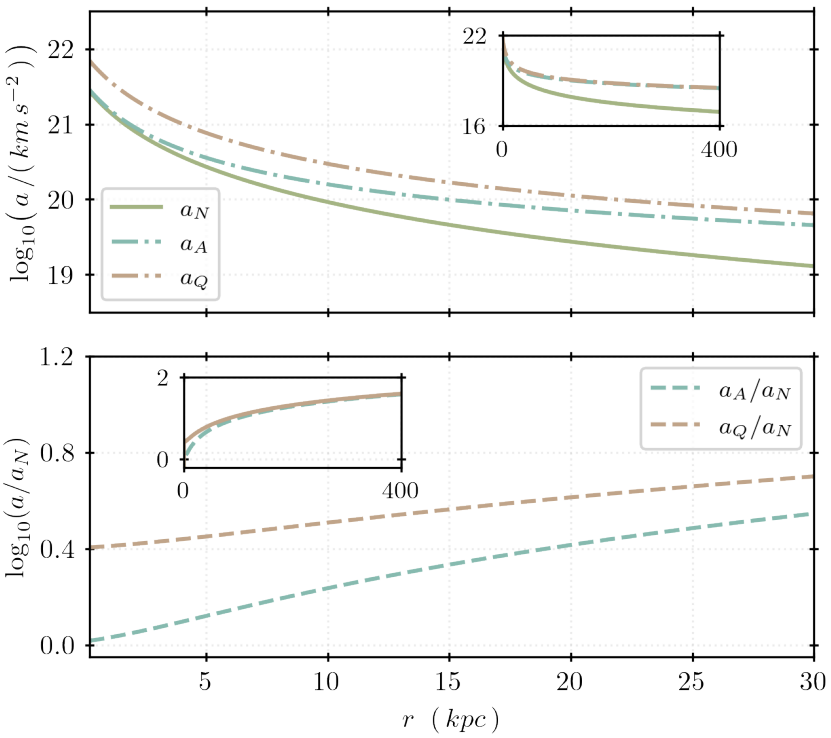

Figure 4.6: Acceleration obtained with `solve_bvp` under boundary value conditions, compared with the analytical Hernquist acceleration.

The Neumann formulation yields solutions that closely match the analytical profiles across the entire radial domain, with smaller deviations near the edges compared to the initial value formulation. This makes the Neumann approach the preferred choice for subsequent MONDian integrations. In particular, the best solution is given by Neumman (BCP) AQUAL.

For AQUAL, the acceleration exhibits the expected transition: Newtonian-like behavior in the inner regions and MONDian modifications at larger radii. QMOND, however, diverges from the Newtonian solution even when forced to recover it at the center.

Overall, both IVP and BCP confirm that AQUAL provides results consistent with previous studies, whereas QMOND remains better suited as an approximation when computational efficiency is required. Having established the general validity of both approaches, we next derive the main dynamical observables, beginning with the velocity dispersion.

4.2.1.3 MOND Observables

From the MONDian potential, we derived the key dynamical observables: the circular velocity, escape velocity, and radial velocity dispersion. These quantities provide the direct link between theory and measurable astrophysical properties.

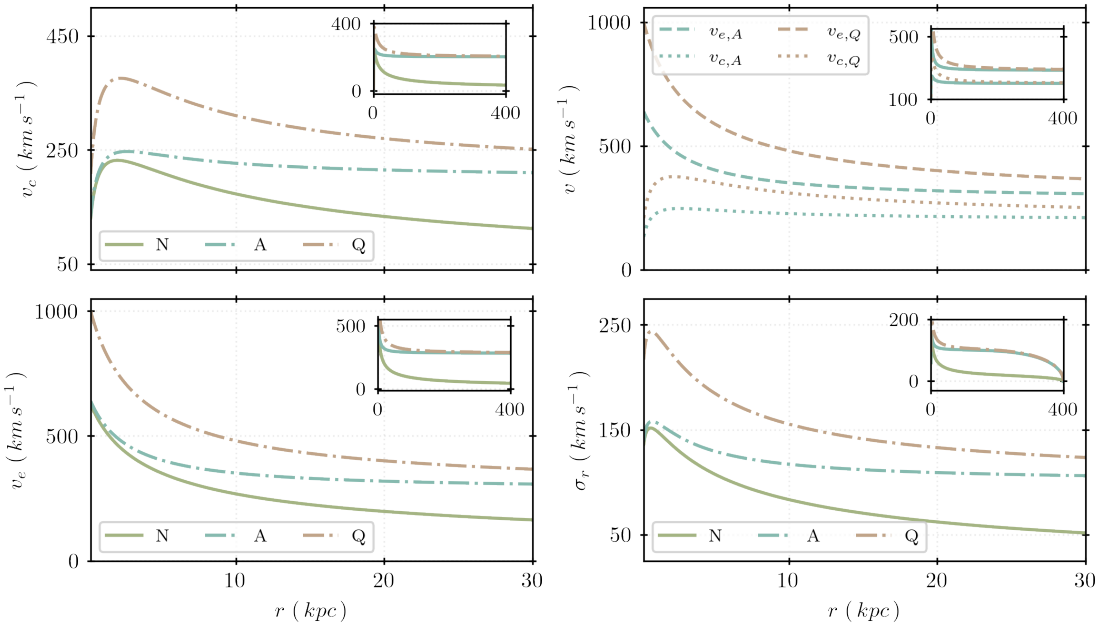

Figure 4.7: Observables derived from the AQUAL solution. The plots show the circular velocity, escape velocity, and velocity dispersion for a representative model. The results reproduce the expected MONDian behavior, particularly the flattening of the rotation curves and the enhancement of dispersions at large radii.

As a first application, we modeled a galaxy-scale system ($M = 10^{11} M_\odot$, $a = 2$ kpc) within the MOND framework. The circular velocity curve exhibited the characteristic

flattening at large radii, while the velocity dispersion remained consistently higher than in the Newtonian case. These results show how MOND reproduces the well-known dynamical discrepancies of galaxies without invoking dark matter.

Overall, MOND predicts three robust signatures: flat rotation curves, higher escape velocities, and enhanced velocity dispersions. Importantly, the QMOND result form has a similar tendency to those obtained from the full AQUAL solver, as both rely on the same interpolation function $\mu(x)$. This consistency validates QMOND as a reliable, faster alternative for parameter-space exploration.

4.2.2 Parameter Exploration

The analysis was then extended to parameter values representative of spheroidal galaxies, to enable future comparisons of the model across a broad range of systems. The parameter space spanned total masses M between 10^9 and $5 \times 10^{10}\, M_\odot$ and scale radii a between 6 and 12 kpc. Solutions were computed on a uniform radial grid up to 10 kpc, with integrations extended to $1000\, a$ to approximate infinity.

The results confirmed the robustness of MOND across this parameter space: rotation curves consistently flattened at large radii, escape velocities remained higher than in the Newtonian case, and velocity dispersions declined more slowly, sustaining random stellar motions in the outskirts. These behaviors provide testable predictions for systems where MOND effects are expected to be evident.

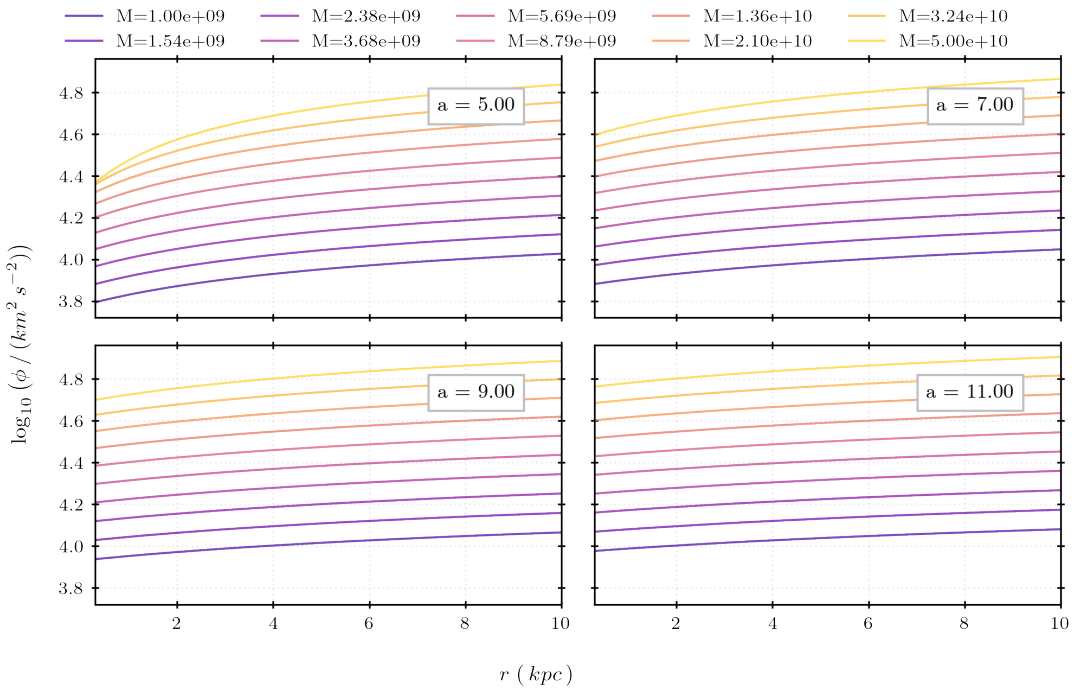

Figure 4.8: MONDian potential profiles for different values of mass M and scale radius a, computed with the AQUAL BCP solver.

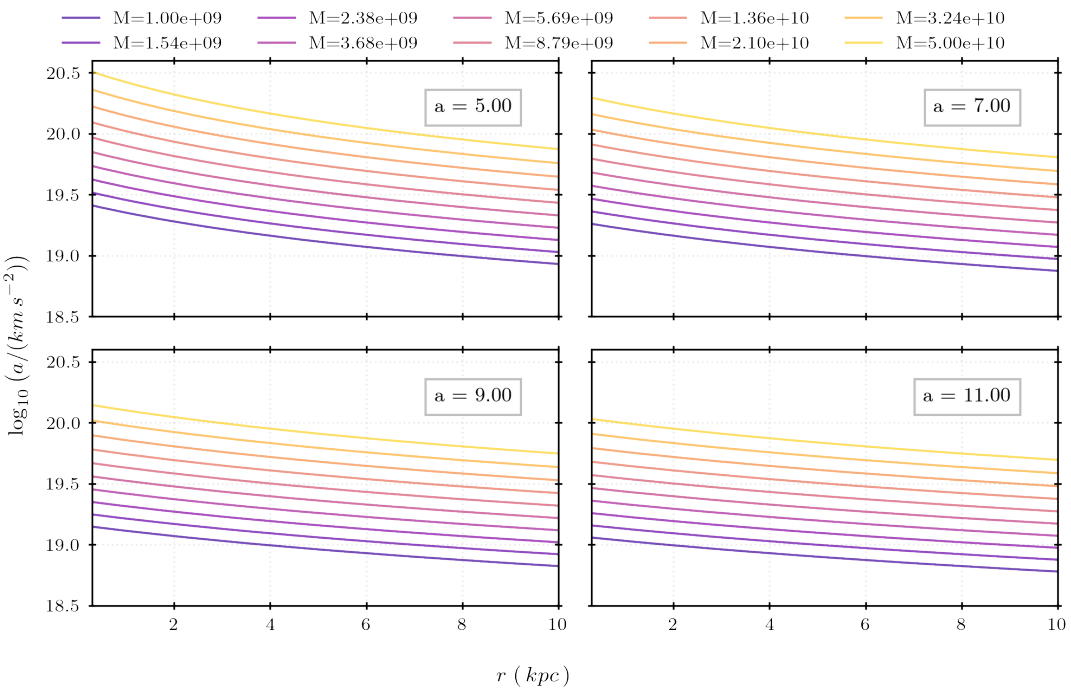

Figure 4.9: MONDian acceleration profiles for different values of mass M and scale radius a, computed with the AQUAL BCP solver.

Taken together, these results establish a coherent picture: both AQUAL and QMOND reproduce the essential MONDian predictions across the parameter space, with AQUAL BCP being the best one. This coherent behavior reinforces the consistency of the framework and sets the stage for discussing its broader implications in the context of modified gravity theories.

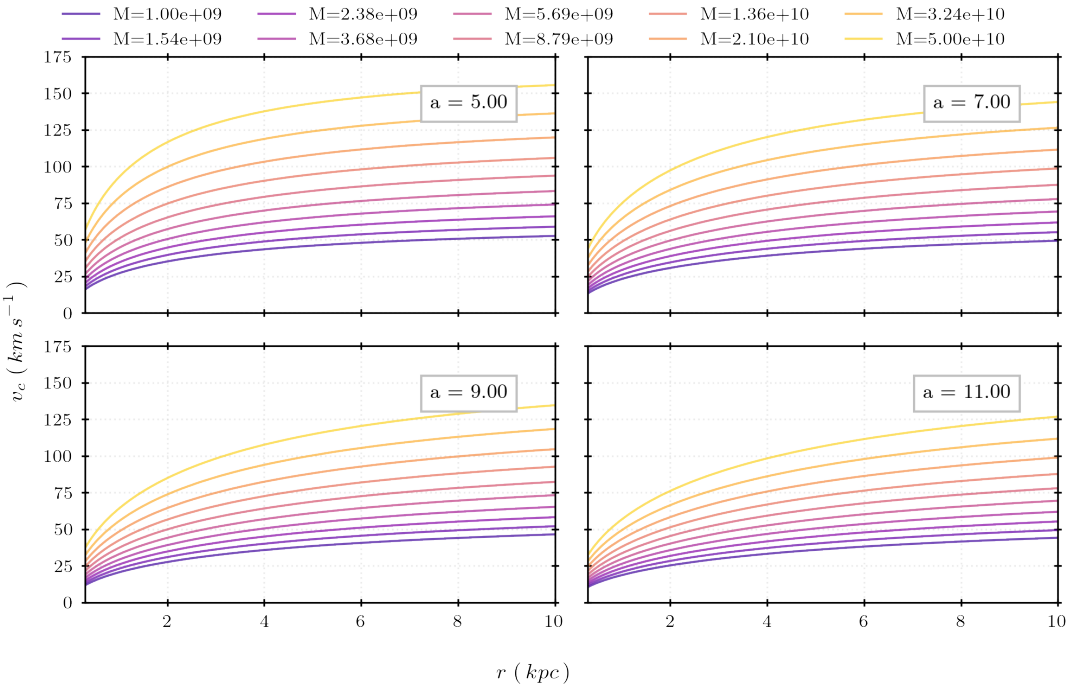

Figure 4.10: Circular velocity curves under MOND for different values of mass M and scale radius a. The flattening at large radii is a robust MONDian feature.

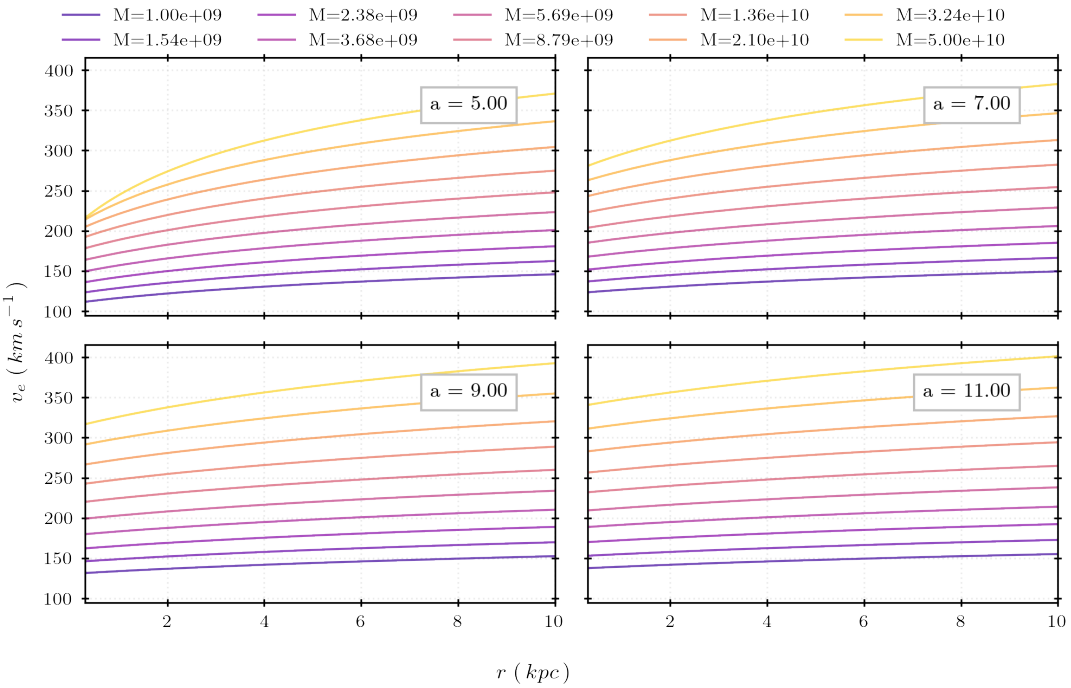

Figure 4.11: Escape velocity profiles under AQUAL BCP for different values of mass M and scale radius a. MOND predicts consistently higher values compared to Newtonian gravity.

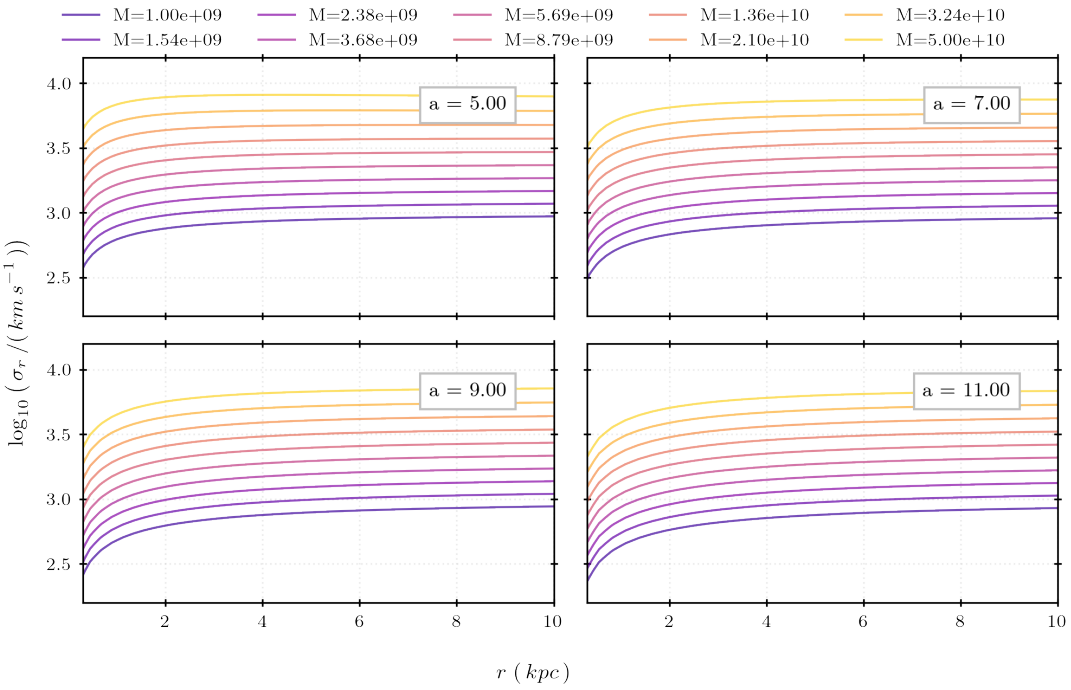

Figure 4.12: Radial velocity dispersion profiles under AQUAL BCP for different values of mass M and scale radius a. The slower decline with radius highlights MOND's ability to sustain random motions in the outskirts of stellar systems.

5

Future Work and Recommendations

This study establishes a numerical framework to investigate the dynamics of globular clusters under Newtonian and MONDian gravity. While the results provide meaningful insights, the work opens several avenues for refinement, expansion, and observational validation. The following subsections outline specific improvements to the methodology, directions for further simulations, and the connection to upcoming comparisons with observational data from *Gaia* DR3.

5.1 Possible Improvements and Next Steps

Several strategies can enhance the current modeling framework:

- **Higher-Order Differentiation Schemes:** Increasing the order of finite-difference formulas beyond the five-point stencil can improve numerical precision, especially near the boundaries.
- **Refined Interpolation Techniques:** Employing higher-degree spline interpolation in place of linear interpolation may suppress numerical oscillations in the computed observables.
- **Parallelization:** Implementing parallel computing techniques can accelerate the iterative solver, enabling exploration of larger and finer parameter spaces within feasible computational times.

5.2 Further Simulations and Observational Comparisons

An important next step involves expanding the parameter space explored, particularly:

- Testing other forms of the $\mu(x)$ interpolation function.

- Simulating non-spherical mass distributions to match more accurately the vast majority of galaxies and globular clusters.
- Including external field effects (EFE) for more realistic modeling of the cluster's environment within the Milky Way.

The most critical task involves a direct comparison between simulated observables and kinematic data from *Gaia* DR3, which will provide a decisive test of MOND predictions against Newtonian expectations.

5.3 Expected Comparison with Gaia DR3

The simulations indicate that MONDian models produce higher velocity dispersions and escape velocities at large radii than Newtonian models without dark matter. Upcoming *Gaia* DR3 observations will provide a direct test of these predictions.

An agreement would provide support for MOND as a possible framework for globular cluster dynamics. In contrast, discrepancies would point either to the limitations of the theory or to the need for more detailed models that incorporate anisotropy, external fields, or tidal effects.

6

Conclusion

This thesis developed and tested a numerical framework to compare Newtonian and MONDian gravities, focusing on the AQUAL and QMOND formulations in galactic ranges. The modeling assumed a spherically symmetric mass distribution described by the Hernquist profile, and the gravitational potential was solved numerically using finite-difference methods combined with an iterative implementation of the AQUAL Poisson equation.

The framework was first validated by solving the Newtonian Poisson equation, confirming excellent agreement with the analytical Hernquist solution. Building on this validation, an iterative solver was implemented for AQUAL, initialized with a QMOND-based guess and refined through successive integrations until convergence. The method demonstrated stability, accuracy, and consistency across a wide parameter space of mass and scale radius values.

From the converged MONDian potentials, we derived key dynamical observables, including the circular velocity, escape velocity, and radial velocity dispersion. The results consistently showed stronger potentials, flatter rotation curves, higher escape velocities, and enhanced dispersions compared to Newtonian predictions. These outcomes align with MOND's theoretical expectations in the low-acceleration regime and reproduce features traditionally attributed to dark matter halos.

A direct comparison between AQUAL and QMOND highlighted their complementary roles. QMOND provides a computationally inexpensive alternative that captures the main MONDian features, making it suitable for large-scale parameter exploration. AQUAL, while more computationally demanding, delivers higher accuracy and serves as a benchmark for reliability. The relaxation method used here could also be optimized further, for example, through an implementation in C, to reduce runtime and make the AQUAL solver more efficient.

An important strength of this framework is its broad applicability. Because the model depends only on two parameters—the total mass M and the scale radius a—it can be adapted to a wide variety of stellar systems, from massive galaxies to dwarf

spheroidals and globular clusters. This flexibility makes it a powerful tool for exploring MOND predictions across multiple astrophysical environments.

While the present results confirm MOND's internal consistency and predictive power, they remain theoretical. The essential next step is to confront these predictions with observational data. In particular, applying this framework to systems such as the Fornax dwarf galaxy and Omega Centauri, using proper motions and velocity dispersions from Gaia DR3, will provide a decisive test of MOND's viability as an alternative to dark matter in bounded stellar systems.

In summary, this study established a robust computational approach for testing modified gravity theories in galaxies and beyond. The findings demonstrate that MOND, and specifically the AQUAL formulation, can reproduce many of the kinematic signatures usually ascribed to dark matter, offering a compelling framework for further investigation in both numerical simulations and observational astrophysics.

This page intentionally left blank.

Bibliography

Abraham, R. G. (1998). "Perspectives in Physical Morphology". In: arXiv: astro-ph/9809131 [astro-ph]. URL: https://arxiv.org/abs/astro-ph/9809131.

Andernach, Heinz and Fritz Zwicky (Nov. 2017). "English and Spanish Translation of Zwicky's (1933) The Redshift of Extragalactic Nebulae". In: *arXiv e-prints*, arXiv:1711.01693, arXiv:1711.01693. DOI: 10.48550/arXiv.1711.01693. arXiv: 1711.01693 [astro-ph.IM].

Bekenstein, J. and M. Milgrom (Nov. 1984). "Does the missing mass problem signal the breakdown of Newtonian gravity?" In: *Astrophysical Journal* 286, pp. 7–14. DOI: 10.1086/162570.

Bekenstein, J. D. (2006). "The modified Newtonian dynamics—MOND and its implications for new physics". In: *Contemporary Physics* 47.6, pp. 387–403. DOI: 10.1080/00107510701244055. URL: https://doi.org/10.1080/00107510701244055.

Bekenstein, Jacob D. (Oct. 2004). "Relativistic gravitation theory for the modified Newtonian dynamics paradigm". In: *Physical Review D* 70.8, 083509, p. 083509. DOI: 10.1103/PhysRevD.70.083509. arXiv: astro-ph/0403694 [astro-ph].

Bertone, Gianfranco, Dan Hooper, and Joseph Silk (Jan. 2005). "Particle dark matter: evidence, candidates and constraints". In: *Physics Reports* 405.5-6, pp. 279–390. DOI: 10.1016/j.physrep.2004.08.031. arXiv: hep-ph/0404175 [hep-ph].

Binney, James and Scott Tremaine (2008). *Galactic Dynamics*. 2nd ed. Princeton, NJ: Princeton University Press.

Famaey, Benoit and Stacy S. McGaugh (2012). "Modified Newtonian Dynamics (MOND): Observational Phenomenology and Relativistic Extensions". In: *Living Reviews in Relativity* 15.10. DOI: 10.12942/lrr-2012-10. URL: https://doi.org/10.12942/lrr-2012-10.

Hernquist, Lars (June 1990). "An Analytical Model for Spherical Galaxies and Bulges". In: *Astrophysical Journal* 356, p. 359. DOI: 10.1086/168845.

Lüghausen, Fabian, Benoit Famaey, and Pavel Kroupa (June 2014). "Phantom of RAMSES (POR): A new Milgromian dynamics N-body code". In: *Canadian Journal of Physics* 93, pp. 232–241. DOI: 10.1139/cjp-2014-0168.

Milgrom, M. (July 1983). "A modification of the Newtonian dynamics as a possible alternative to the hidden mass hypothesis." In: *Astrophysical Journal* 270, pp. 365–370. DOI: 10.1086/161130.

Milgrom, Mordehai (Oct. 2009). "MOND effects in the inner Solar system". In: *Monthly Notices of the Royal Astronomical Society* 399.1, pp. 474–486. DOI: 10.1111/j.1365-2966.2009.15302.x. arXiv: 0906.4817 [astro-ph.CO].

Mo, H., F. van den Bosch, and S. White (2010). *Galaxy Formation and Evolution*. Galaxy Formation and Evolution. Cambridge University Press. ISBN: 9780521857932. URL: https://books.google.ca/books?id=Zj7fDU3Z4wsC.

Oort, J. H. (Aug. 1932). "The force exerted by the stellar system in the direction perpendicular to the galactic plane and some related problems". In: *Bulletin of the Astronomical Institutes of the Netherlands* 6, p. 249.

Rubin, V. C., W. K. Ford Jr., and N. Thonnard (Nov. 1978). "Extended rotation curves of high-luminosity spiral galaxies. IV. Systematic dynamical properties, Sa -> Sc." In: *Astrophysical Journal Letters* 225, pp. L107–L111. DOI: 10.1086/182804.

Schumann, Marc (Aug. 2019). "Direct detection of WIMP dark matter: concepts and status". In: *Journal of Physics G: Nuclear and Particle Physics* 46.10, p. 103003. DOI: 10.1088/1361-6471/ab2ea5. URL: https://dx.doi.org/10.1088/1361-6471/ab2ea5.

Zhao, HongSheng (Dec. 2001). "Are Omega Centauri and G1 like massive globular clusters the remnant cores of infalling dwarf galaxies? – Dynamical constraints". In: *arXiv e-prints*, astro-ph/0112094, astro–ph/0112094. DOI: 10.48550/arXiv.astro-ph/0112094. arXiv: astro-ph/0112094 [astro-ph].

Zwicky, F. (Jan. 1933). "Die Rotverschiebung von extragalaktischen Nebeln". In: *Helvetica Physica Acta* 6, pp. 110–127.

This page intentionally left blank.